JOURNAL OF MATERIALS SCIENCE 14 (1979) 1473–1494

Hertzian fracture of Pyrex glass under quasi-static loading conditions

H. CONRAD, M. K. KESHAVAN, G. A. SARGENT
Metallurgical Engineering and Materials Science Department, University of Kentucky, Lexington, Kentucky 40506, USA

Hertzian fracture tests were conducted using an Instron on Pyrex glass specimens with various surface conditions, including lubricants, employing steel, Al_2O_3, WC and Pyrex glass indentors of 0.79 to 12.7 mm radius under ambient air and high vacuum environments at cross-head speeds of 8.5×10^{-6} to 2.1×10^{-4} m sec^{-1}. The results were not in strict accord with Auerbach's law, nor any of the existing energy-balance Hertzian fracture theories. Rather, they indicated that surface roughness and friction modified the Hertz stress field so that the maximum tensile stress at the surface occurred outside the contact circle. Further, they indicated that Hertzian fracture occurred by the direct, unstable growth into a cone crack of a pre-existing flaw at the displaced site of the maximum tensile stress, the flaw size responsible for the fracture decreasing with decrease in ball size (contact radius). Once a cone crack occurred, its length and growth were described reasonably well by Roesler's theory; however, his constant appears to be too high by a factor of about 5. A surface energy of ~ 4 J m^{-2} was derived from bend tests on specimens similar to those used in the Hertzian fracture tests. Using this value, the crack sizes which lead to fracture were estimated to range between 0.6 and 3.5 μm for the conditions investigated here. The increase in the critical load for Hertzian fracture with indentation velocity was concluded to be due to kinetic effects of water vapour acting at the tip of the crack.

1. Introduction

The Hertzian fracture test, in which a relatively hard sphere is loaded onto a flat specimen, is of both scientific and technological interest. From a scientific standpoint, the test can yield information on the fracture behaviour of brittle materials and the related surface energy and fracture toughness values. From a technological viewpoint, the important event in such phenomena as abrasion, wear and erosion of brittle materials by hard solid particles appears to be related to the brittle fracture produced by individual particles, which can be considered as either blunt (spherical) or sharp (pointed) indentors.

The stresses beneath a spherical indentor loaded onto a flat plate were first calculated by Hertz [1]. Even though the stress state is complex, it is well defined up to the point of fracture in a perfectly elastic–brittle specimen. Experimentally, the first evidence of fracture is generally a ring crack at the specimen surface located near (generally outside) the contact circle of the spherical indentor on the flat surface, where the radial tensile stress is a maximum. With further increase in load, the ring crack develops into a cone crack, the profile of which follows approximately the contour of the minimum principal stress, σ_{33}, extending beneath the surface of the specimen; this contour makes an angle of approximately 22° with the surface.

Studies of Hertzian ring crack formation by a number of investigators have established that, within a certain indentor size range, the critical load to produce the crack is approximately proportional to the indentor radius. This relationship has been termed Auerbach's law [2]. Roesler [3]

first pointed out that a number of additional relationships which had been reported for Hertzian ring crack formation in glass are also in accord with Auerbach's law. Furthermore, he showed that Auerbach's law is in accord with an energy scaling concept, namely that the total elastic strain energy of the indentor and specimen divided by the area of contact is a constant. Subsequent theoretical considerations of Hertzian fracture in terms of fracture mechanics by Frank and Lawn [4] and later by Lawn and co-workers [5–7] yielded Auerbach's law for certain ratios of pre-existing surface flaw size to contact radius. Once a ring crack had formed, their theory included the analysis of Roesler [8] as a description of its growth into a well-defined cone crack.

Work by Lawn and Wilshaw and their co-workers [4–7, 9–13] has indicated that reasonable accord exists between experimental observations on Hertzian ring crack formation and growth and the theories developed by them. However, additional information on a number of features relating to Hertzian ring crack formation is needed before these theories can be completely accepted. Of special interest to the present authors were: (a) the statistical nature of the critical load to produce the ring crack, (b) the influence of the speed of testing, (c) the influence of indentor material, size and surface condition, (d) the effect of surface condition of the specimen including lubrication, (e) the ratio of ring crack radius to contact radius, and (f) the effect of the environment. This investigation considered the effects of the above factors on the Hertzian fracture of Pyrex glass, since only limited studies had been carried out on this type of glass. It will be seen that the results are not in strict accord with the original Frank–Lawn–Wilshaw theories of Hertzian fracture. A factor neglected in their theories which appears to be highly important is the roughness and friction between the indentor and the specimen.

2. Hertz equations

The following Hertzian elastic contact equations are important to the analysis of the results of the present study:

$$a^3 = \frac{4kPR}{3E} \tag{1}$$

where

$$k = \frac{9}{16}\left[(1-\nu^2)+(1-\nu'^2)\frac{E}{E'}\right], \tag{2}$$

and R is the radius of the contacting sphere, a the radius of the circular elastic contact area, P the applied normal load, E and E' the Young's modulus of the specimen and sphere, respectively, and ν and ν' their respective Poissons ratios. The distance of mutual approach, Z, between the contacting bodies is given by

$$Z^3 = \left(\frac{4k}{3E}\right)^2 \frac{P^2}{R}. \tag{3}$$

In addition to these three basic equations, we will be interested in the tensile stress, σ_{rr}, which acts radially in the surface of the specimen. The maximum tensile stress occurs at the contact circle and decreases away from the periphery according to

$$\sigma_{rr} = \left(\frac{1-2\nu}{2}\right)\frac{P}{\pi a^2}\left(\frac{a}{r}\right)^2 = \left(\frac{1-2\nu}{2}\right)p_0\left(\frac{a}{r}\right)^2, \tag{4}$$

where r is the radial distance from the point of contact and $P/\pi a^2$ is the average pressure p_0. Also, of interest is the contact time, t_c, between the indentor and the specimen up to the point of fracture, which for the constant cross-head speed testing employed in the present investigation becomes

$$t_c = \frac{Z}{\dot{Z}} = \left(\frac{4k}{3E}\right)^{2/3}\left(\frac{P^2}{R}\right)^{1/3}\frac{1}{\dot{Z}}, \tag{5}$$

where $\dot{Z}$ is the cross-head velocity.

The testing speeds and contact times considered in this investigation are well within the range where quasi-static conditions prevail [12, 13], and the equilibrium equations of elasticity are expected to provide an adequate description of the system.

3. Materials and test procedure

3.1. Target

The target (specimen) material for all of the present tests was Corning 7740 Pyrex glass plate, generally 50 mm × 50 mm × 10 mm thick, of the composition and properties listed in Table I. Tests were conducted on the as-received (ground-and-polished) surface and after the following treatments had been given to this surface: (a) annealing, (b) abrasion, (c) anneal plus abrasion, (d) anneal plus abrasion plus anneal, and (e) etching for various times in 55% HF. Annealing consisted of slowly heating the specimen in air to 460° C, holding at this temperature for 2½ h, and then slowly cooling

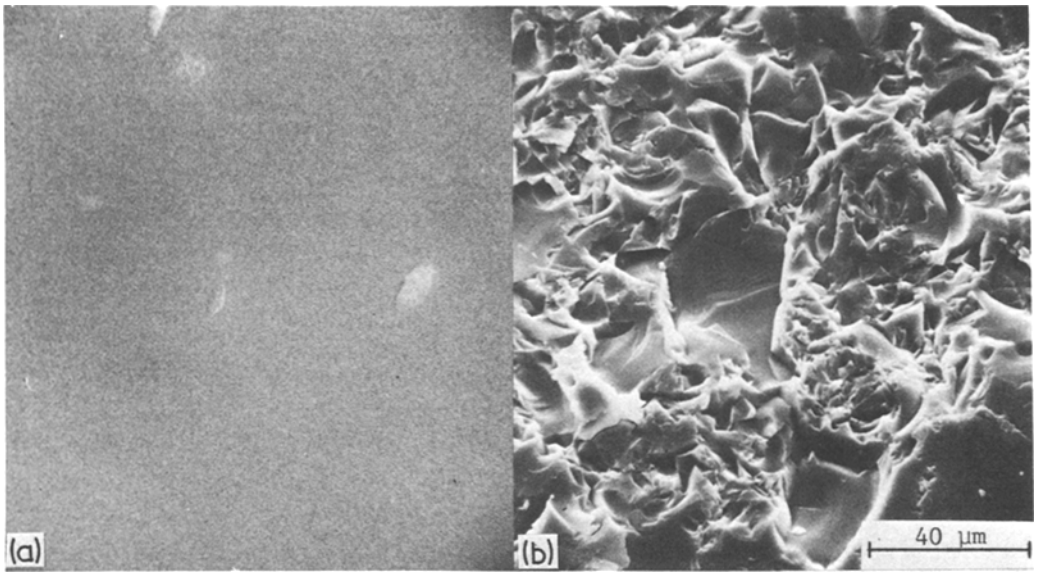

Figure 1 SEM micrographs of the surface of the Pyrex glass specimen (a) initial as-received (ground-and-polished), (b) abraded with 400 grit SiC.

to room temperature. Abrasion was by hand polishing using a water slurry of 400 grit SiC particles on a glass plate, similar to the procedure employed by Langitan and Lawn [6]. The maximum depth of crack produced by this abrasive treatment was determined by them to be about 18 μm [6].

Scanning electron micrographs (SEM) of the surface structure of the as-received and abraded surfaces are presented in Fig. 1. Etching of these surfaces in HF for 20 min yielded the network structure shown in the optical micrograph of Fig. 2. A similar network was observed by Argon [14] on Pyrex glass exposed to sodium vapours; he considered the network to be that of surface cracks.

3.2. Indentors

Most of the tests were conducted using hardened and polished chrome-alloy steel balls ranging from 0.8 to 12.7 mm radius. Limited studies were also performed with polished aluminium oxide (Al_2O_3), tungsten carbide (WC) and Pyrex glass spheres within the same size range as the steel balls. Some tests were also conducted using steel balls which had been roughened by sandblasting for a few seconds. The composition and properties of the various balls are given in Table II. Unless otherwise stated, the results presented below will be for the as-received, polished surface of the various indentors.

TABLE I Composition and properties of the target (specimen). Material: Corning ground-and-polished Pyrex 7740 glass plate (borosilicate glass)

(a) Composition (wt%) [34]			
SiO_2	Al_2O_3	Na_2O	B_2O_3
81	2	4	12
(b) Properties [25]*		[25]	
Young's modulus E ($GN\,m^{-2}$)	Poissons ratio ν	Hardness H Knoop R_c	Surface energy γ_s ($J\,m^{-2}$)
6.37×10^1	0.2	418 42 448† 44†	4.0

* Industrial Tectronics, Inc, Ball Division, PO Box 1128 Ann Arbor, Michigan (supplier).
† Present authors.

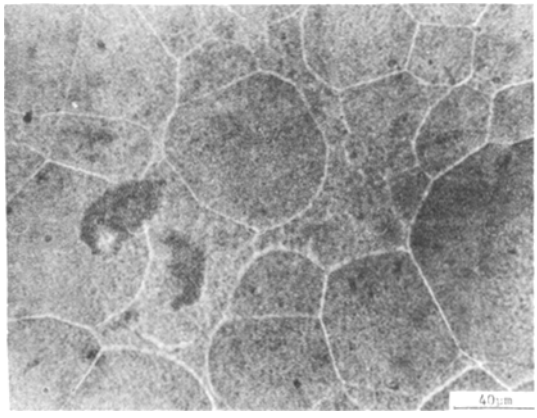

Figure 2 Optical micrograph showing the network on the surface of a Pyrex glass specimen following etching in 55% HF for 20 min.

TABLE II Composition (wt%) and properties of the indentors

(a) Composition*

1. Steel: chrome alloy steel, AISI 52100 steel

C	Mn	P	S	Cr	Si	Ni	Cu	Mo
0.95–1.10	0.25–1.45	0.025	0.025	1.3–1.6	0.2–0.35	0.35	0.25	0.08

2. Aluminium Oxide: 99.5 wt% Al_2O_3
3. Tungsten carbide: 93.5–94.5 wt% WC
   5.5– 6.5 wt% Co
4. Pyrex glass: see Table I.

(b) Mechanical properties†‡

Material	Young's modulus E' (10^2 GN m^{-2})	Shear modulus μ' (10^1 GN m^{-2})	Poissons ratio ν'	Hertzian constant§ k	Friction constant§ K	Rockwell hardness
Steel	2.07	7.96	0.30	0.6974	0.4515	63–66 (C-Scale)
Al_2O_3	3.59	14.59	0.23	0.6346	0.5339	81(N-Scale, 45kg)
WC	7.77	26.87	0.26	0.5894	0.6330	91–92 (A-Scale)
Pyrex glass	0.64	2.65	0.20	1.080	0	44 (C-Scale)

* SKF Industries, Inc, Suite 3 Colony Square, 7770 Cooper Road, Cincinnati, Ohio 42542 (supplier).
† Industrial Tectronics Inc, Ball Division PO Box 1128, Ann Arbor, Michigan (supplier).
‡ See Table I.
§ $k = \frac{9}{16}\left[(1-\nu^2) + (1-\nu'^2)\frac{E}{E'}\right]$ and $K = \frac{[(1-2\nu)/\mu] - [(1-2\nu')/\mu']}{[(1+\nu)/\mu] + [(1-\nu')/\mu']}$, where μ is the shear modulus and the unprimed symbols refer to the Pyrex glass specimen.

3.3. Test procedure

The present tests were conducted under ambient conditions, i.e. in air and at atmospheric pressure (except when otherwise noted), using a bench model Instron testing machine. The balls and specimen were cleaned in acetone prior to each test. The specimen was clamped to the x–y stage of an optical microscope, which was mounted onto the moving cross-head of the Instron. The arrangement was such that the contact surface of the glass could be observed with the microscope at $\times 20$ through the back of the specimen. The jig holding the ball indentor was placed onto the compression load cell attached to the base plate of the testing machine. The specimen was pressed against the indentor at a constant cross-head speed in the range of 8.5×10^{-6} to 2.1×10^{-4} m sec^{-1}, the behaviour being continually observed under the microscope from the time of contact until a full ring crack had developed, at which instant the machine was generally stopped and subsequently unloaded. The ring crack always appeared to start at one point and then proceed to form its circumference. In the case of the as-received and the etched surfaces, this occurred in less than 1 sec; for the abraded surface the development of the ring took from 1 to 12 sec and could be easily followed under the microscope, the load continuing to increase as the crack developed. A total of 20 to 40 such tests were generally conducted for each ball size and test condition.

The critical load, P_c, was taken as the load for the full development of the ring crack. Fig. 3 shows typical cracks formed at P_c on the various specimen surfaces as seen through the microscope at $\times 20$. Not shown here is that for the annealed-plus-abraded-plus-annealed surface; its appearance being the same as that of Fig. 3e. In each case a cone crack occurred along with the ring crack, although for the as-received surface the cone portion was barely detectable. Upon unloading, the ring-and-cone crack generally disappeared for the ground-and-polished surfaces; it was only faintly visible, if at all, for the abraded surfaces, but remained clearly visible for the etched surfaces.

4. Experimental results

4.1. Statistical nature of the critical load to produce Hertzian fracture

The critical load, P_c, at which a crack formed and the radius, r^*, of the ring crack at the surface were determined for each of the 20 to 40 tests conducted with each size of the various indentor materials and for the various surface conditions. In

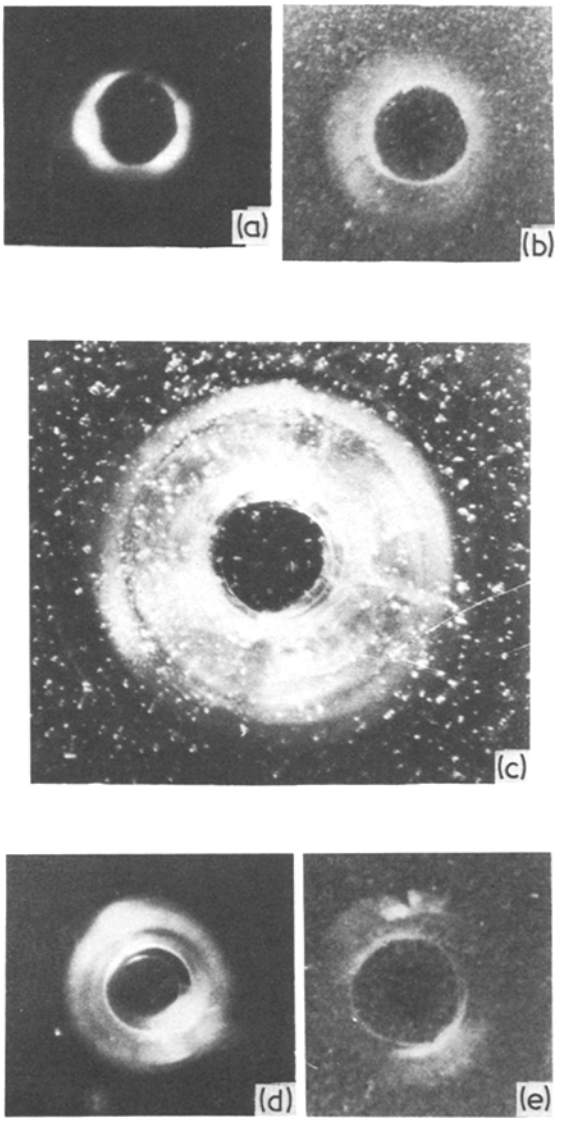

Figure 3 Typical cracks at the critical load P_c (3.18 mm radius steel ball) observed through the back side of the specimen at × 20. (a) Initial as-received surface; P_c = 128 N, (b) abraded with 400 grit SiC; P_c = 211 N, (c) etched in 55% HF for 2 min; P_c = 716 N, (d) annealed for $2\frac{1}{2}$ h at 460° C; P_c = 208 N, and (e) annealed plus abraded with 400 grit SiC; P_c = 193 N. (The figure is reproduced here at 90% original size.)

keeping with the fracture of brittle materials, P_c exhibited appreciable scatter; so the results were considered statistically. The procedure generally adopted was to determine the cumulative frequency (probability) f'_F as a function of P_c. This was obtained by arranging the N total values of P_c in increasing order and assigning a number n to each value; f'_F is then given by $n/N + 1$. Some tests were also performed whereby the per cent probability was determined from the fraction of the tests at a given load which resulted in cracks. In these tests the load was increased to a predetermined value a fixed number of times (10 to 20) and the fraction of the tests, f_F, which produced a crack noted. As will be seen below, the value of f_F determined in this manner is in agreement with the cumulative frequency f'_F determined by the more conventional tests.

The results obtained in the conventional tests (increasing the load to fracture) for the various size steel indentors on the as-received and on the abraded specimen surfaces are presented in Fig. 4, which is a plot of cumulative frequency f'_F (probability) versus P_c. Similar curves were obtained using the other ball materials. To be noted from Fig. 4 is that the scatter in the values of P_c increases markedly with ball size for the as-received surface. An increase in scatter also occurs for the abraded surface but to a much smaller degree. The annealing treatment increased the scatter for the initial as-received surface but decreased it slightly for the previously abraded surface. The scatter in P_c also increased upon etching the surface. The effect of surface condition of the specimen on the statistical distribution of P_c for a constant indentor radius is illustrated in Fig. 5.

The effect of cross-head velocity on the probability for fracture versus P_c curve for a given ball size is shown in Fig. 6. It is evident here that the scatter increases with loading rate, the effect being greater for the as-received specimen surface compared to the abraded surface.

Fig. 7 shows that the results obtained in the second type of test (i.e. for constant fixed loads) are in statistical accord with those for the more common test method. Hence, to study the influence of test variables on the Hertzian fracture, the value of the load for a fracture probability (cumulative frequency) of 0.5 is here taken as a representative parameter of the fracture behaviour in curves such as those of Figs. 4 to 6. This load is designated $P_{c,0.5}$. Similarly, the values of the other parameters to be considered in this paper will be those for a cumulative frequency of 0.5. For simplification, the experimental values of the various parameters will be listed in the written portion of the text without the subscript 0.5, it being understood that they refer to a cumulative frequency of 0.5 unless otherwise stated. The subscript will, however, be included in the figures and

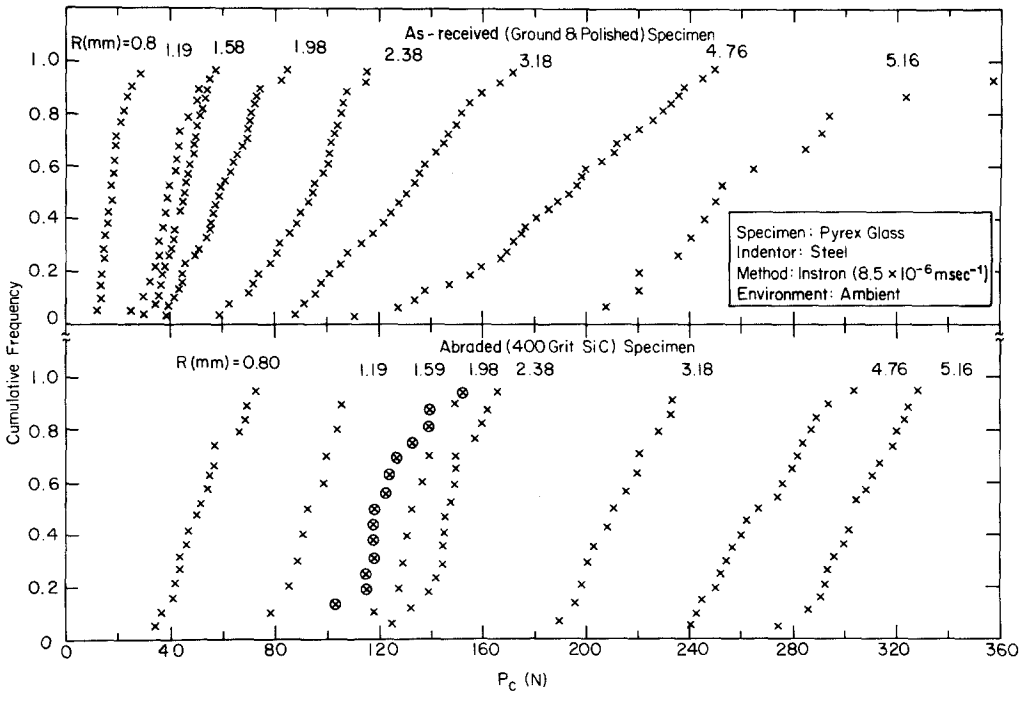

Figure 4 Cumulative frequency (probability) versus the critical load P_c for Hertzian fracture of as-received and abraded specimen surfaces.

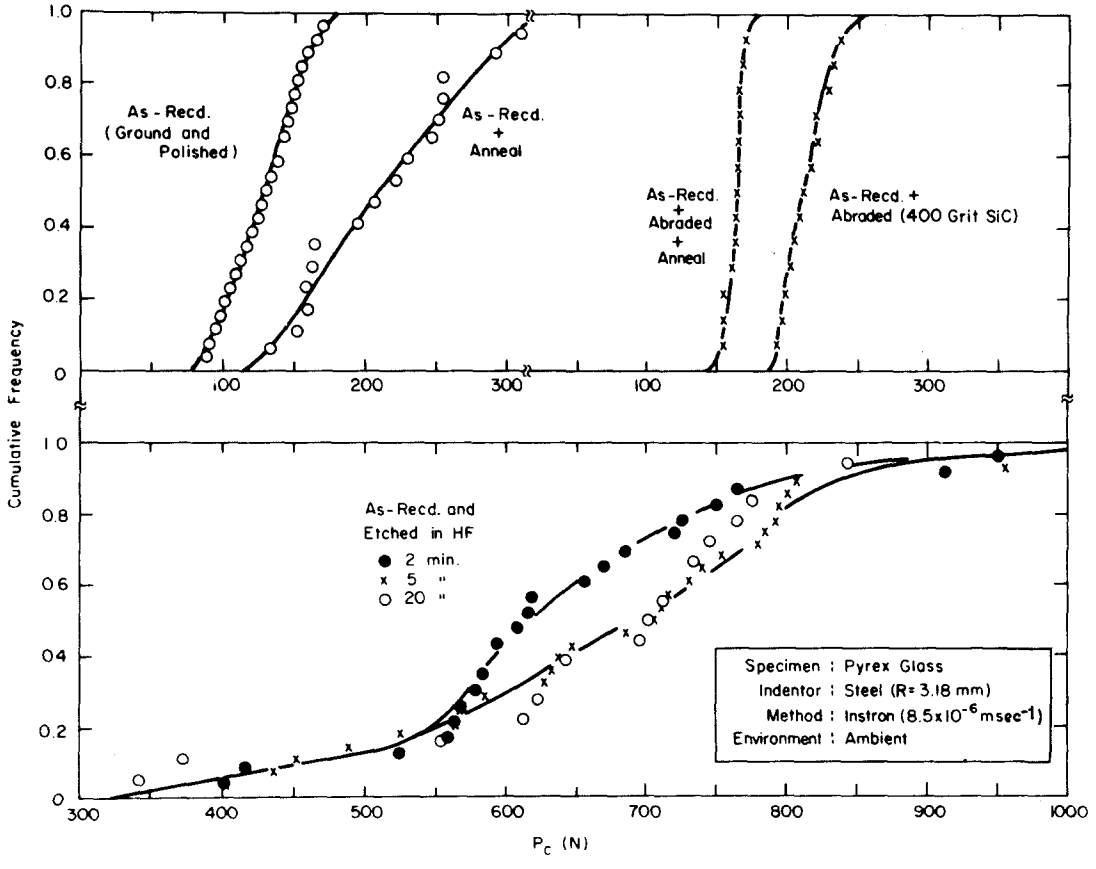

Figure 5 Effect of specimen surface condition on the probability of fracture versus P_c.

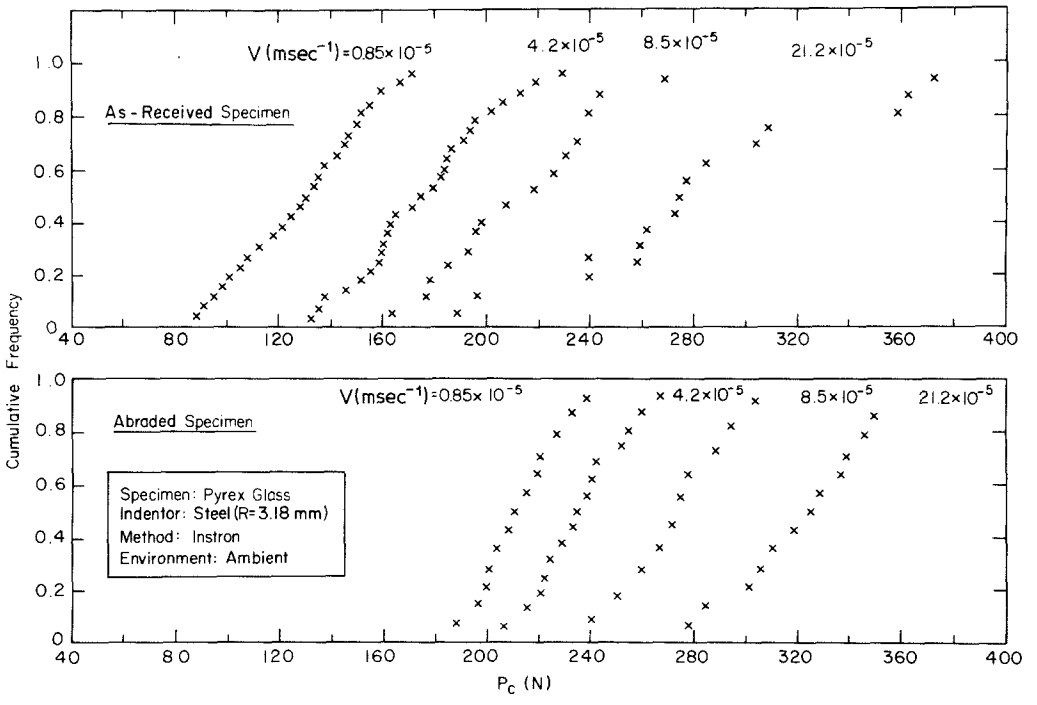

Figure 6 Effect of indentation rate on the probability of fracture versus P_c for as-received and abraded specimen surfaces.

tables. A more detailed analysis of the statistical nature of Hertzian fracture is beyond the scope of this paper and will be treated in a separate paper.

4.2. Indentor size

To check whether the present results conformed to Auerbach's law, the ratio P_c/R is plotted versus the ball radius, R, in Fig. 8. It is here seen that P_c/R varies with indentor size, rather than being a constant as required by Auerbach's law, the value of the ratio increasing with R for the as-received, ground-and-polished specimen surface and decreasing for the abraded surface. The value of P_c/R extrapolated to $R = 0$ increases in the order: as-received, annealed, abraded-plus-anneal, abraded, (etched). Further, there is a tendency for P_c/R to increase upon abrading the steel indentor. The P_c/R ratio tends to decrease with indentor material in the order: steel, (Pyrex glass), Al_2O_3, WC, the effect of indentor material being more pronounced for the ground-and-polished specimen surface than for the abraded surface. The effect of etching on the Hertzian fracture parameters are given in Table III. It is seen that P_c/R increases markedly upon etching, but decreases again for long etching times.

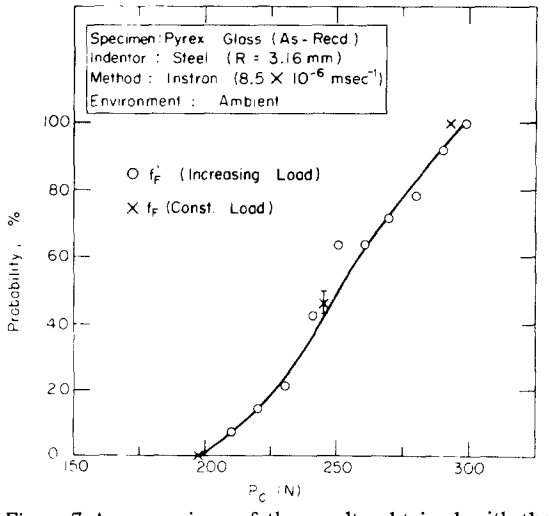

Figure 7 A comparison of the results obtained with the Instron for two conditions of testing: (a) increasing the load until a Hertzian ring crack occurs, yielding the cumulative frequency f_F', and (b) conducting a fixed number of tests (20) at a constant load and noting the fraction f_F which resulted in Hertzian ring cracks.

Log–log plots of P_c versus R yielded reasonably straight lines (see, for example, Fig. 9) suggesting a relationship of the form

$$P_c = AR^n. \tag{6}$$

The values of the constants A and n derived from such plots for various test conditions are given in Table IV.

Worthy of note regarding the results in Fig. 8 is that the ball sizes considered here are within the

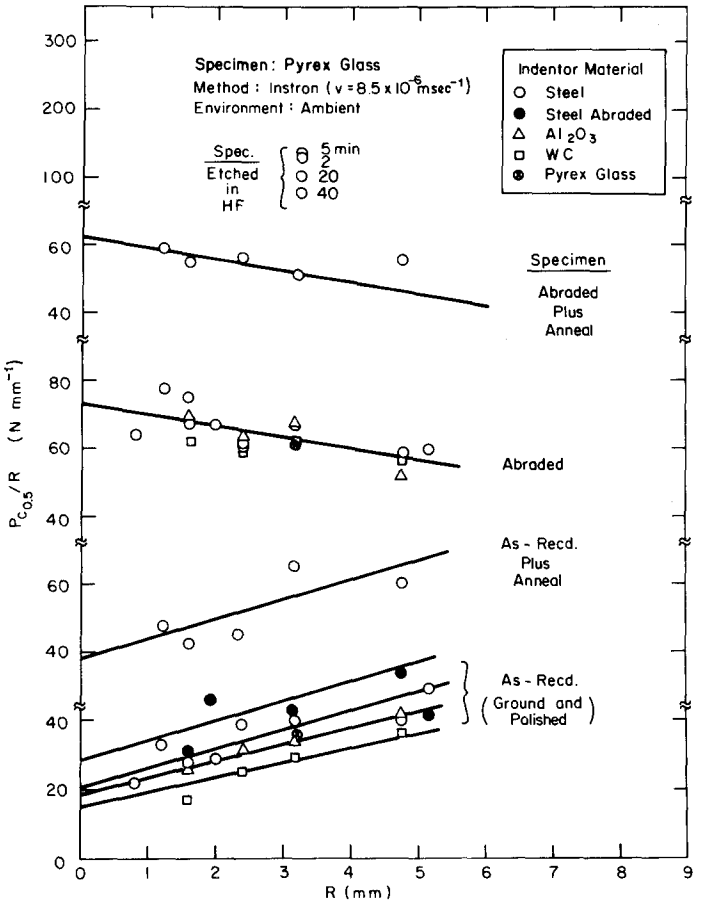

Figure 8 The ratio $P_{c0.5}/R$ versus the ball radius R for various specimen surface conditions and indentor materials.

TABLE III The effect of etching the as-received Pyrex glass surface in 55% HF for various times on the critical load $P_{c0.5}$ for Hertzian fracture using a 3.18 mm radius (R) steel ball and a cross-head speed of 8.5×10^{-6} m sec^{-1}

Etching time (min)	$P_{c0.5}$ (N)	$r^{*\dagger}_{c0.5}$ (mm)	$P_{c0.5}/R$ (N mm^{-1})	t_c (sec)	$\dot{P}_c$ (N sec^{-1})	$r^*_{c0.5}/a_{0.5}$
0	128	0.22	40	2.42	52.7	1.19
2	716	0.39	225	7.62	93.5	1.22
5	740	0.39	233	7.82	94.5	1.19
20	637	0.39	200	7.08	90.0	1.26
40	392	0.32	123	5.12	76.6	1.22

† r^* = ring crack radius.
‡ $\dot{P}_c = P_{c0.5}/t_{c0.5}$.

range where others have found Auerbach's law to be valid for various glasses [3, 6, 7, 15–18]. However, departures from Auerbach's law have also been reported for these sizes by Hamilton and Rawson [17] for the tin-bath surface of float glass and after etching polished plate glass, and by Nadeau [19] for vitreous carbon. Also of interest is that abrading plate-and-float glasses generally leads to both a decrease in scatter of the results and a slight decrease in P_c [6, 9, 20], compared to the increase in P_c observed here for Pyrex glass. Etching of plate glass caused an increase in the critical load [17, 20] and decrease in scatter [20], the latter effect being opposite to that found here for Pyrex glass.

4.3. Indentation rate

It is seen in Fig. 6 that the critical load to cause fracture for a given indentor size increases with the cross-head velocity. Of more pertinent interest is the effect of contact time t_c (Equation 5) and of the average loading rate $\dot{P}_c$ ($= P_c/t_c$) on the value of the ratio (P_c/R) for the various test conditions considered here. A plot of this ratio versus log t_c is

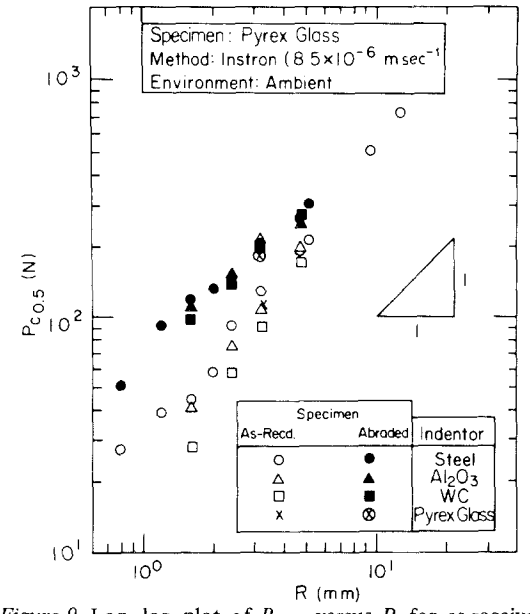

Figure 9 Log–log plot of $P_{c_{0.5}}$ versus R for as-received and abraded surfaces using various indentor materials.

presented in Fig. 10. Included in this plot are the results for a variation in cross-head speed (8.6×10^{-6} to 2.1×10^{-4} m sec^{-1}) with a constant size indentor ($R = 3.18$ mm), and for a range in ball sizes ($R = 0.79$ to 5.16 mm) at a constant cross-head speed (8.5×10^{-6} m sec^{-1}), both of which yield a variation in t_c. It is seen that for the constant indentor size, P_c/R decreases in an approximately linear fashion with log t_c for both the as-received and abraded surfaces. On the other hand, for the variation in t_c due to indentor size, the ratio increases linearly with log t_c for the as-received surface; it however decreases for the abraded surface.

The variation of P_c/R with average loading rate $\dot{P}_c$ is shown in Fig. 11. Here for a constant indentor size, the ratio increases linearly with log $\dot{P}_c$ for both the as-received and abraded surfaces. For the variation in $\dot{P}_c$ due to a change in indentor size, the results for the as-received surface lie on the curve representing the change in cross-head velocity, i.e. P_c/R increases with $\dot{P}_{c,0.5}$. On the other hand, P_c/R for the abraded surface decreases with $\dot{P}_c$ for the variation in $\dot{P}_c$ due to indentor size. Hence, the effects of average loading rate are just the opposite of those obtained for the average contact time in Fig. 10. The results of Figs. 10 and 11 thus indicate that to rigorously check the validity of Auerbach's law, tests with different indentor sizes should be considered for the same contact time or for the same loading rate.

Worthy of note regarding the present results is that Lawn and co-workers [7, 11] also reported that the critical load for Hertzian fracture of plate glass using a constant indentor size decreased with

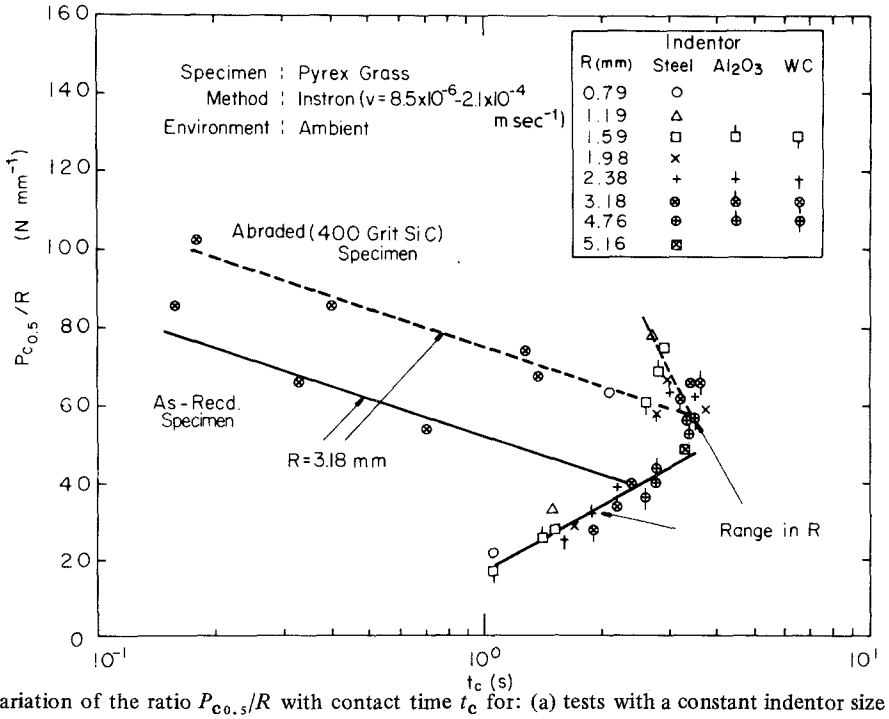

Figure 10 Variation of the ratio $P_{c_{0.5}}/R$ with contact time t_c for: (a) tests with a constant indentor size and different cross-head speeds, and (b) tests at a constant cross-head speed but different sizes of indentor.

TABLE IV Effect of specimen surface condition and ball material and condition on the constants A and n in the equation $P_{co.5} = AR^n$.

Pyrex glass specimen surface condition	Ball material and condition	A (N mm^{-2})	n
As-received (ground-and-polished)	Steel polished	25	1.3
	Steel abraded	32	1.3
	Al_2O_3 polished	21	1.4
	WC polished	14	1.6
As-received + abraded†	Steel polished	70	0.9
	Al_2O_3 polished	70	0.9
	WC polished	66	0.9
As-received + annealed‡	Steel polished	41	1.3
As-received + annealed‡ + abraded†	Steel polished	74	0.9
As-received + annealed‡ + abraded† + annealed	Steel polished	54	1.0

† Abrasion was by hand polishing using a slurry of 400 grit SiC.
‡ Annealing consisted of heating for 2½h at 460° C and slowly cooling.

increase in contact time or with decrease in loading rate for tests in air and water vapour. No significant kinetic effects, however, occurred when the tests were performed under a vacuum ($< 10^{-4}$ N m^{-2}).

4.4. Hertzian cracks

As mentioned above, microscopic observation of the specimen under load indicated that the Hertzian ring crack generally started at one point on its circumference and then proceeded to form the circle (under increasing load for the abraded specimen surface). Typical increases in load and time required for the growth of a complete ring crack in abraded specimens are presented in Table V. Worthy of note here is that the value of P_c/R for the initiation of the cracks in the abraded specimens are only slightly higher than those for the as-received surface (Fig. 8), where the ring crack formed almost instantly. Tillet [15] and

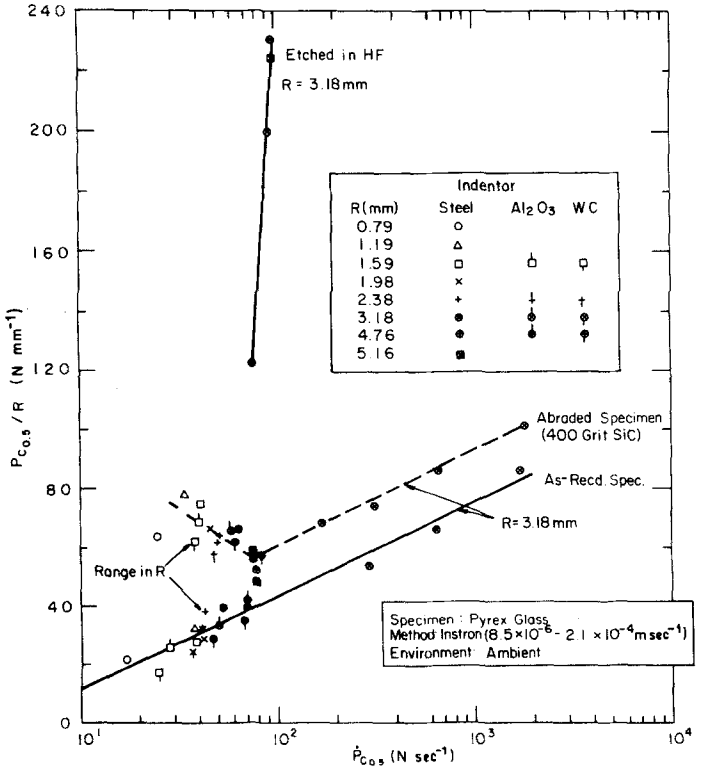

Figure 11 Variation of the ratio $P_{co.5}/R$ with average loading rate $\dot{P}_{co.5} = P_{co.5}/t_c$ for: (a) tests with a constant indentor size and different cross-head speeds, and (b) tests at a constant cross-head speed but different sizes of indentor.

TABLE V The increase in load and time required for the growth of a complete ring crack in abraded (400 grit SiC) Pyrex glass using a 5.26 mm radius steel ball with the Instron ($v = 8.5 \times 10^{-6}$ m sec^{-1}) at ambient conditions

Load at first observation of a crack, P_i (N)	P_i/R (N mm^{-1})	Load at time of complete ring crack, P_c (N)	P_c/R (N mm^{-1})	$P_c - P_i$ (N)	Time for crack to develop, t (sec)
265	50.4	319	60.6	54	11.1
250	47.5	292	55.5	42	6.0
243	46.2	314	59.7	71	7.5
279	53.0	323	61.4	44	6.0
248	47.1	324	61.6	76	12.0

Andrews [21] also reported that the formation of the ring crack did not take place instantaneously. Tillet [15] found that the time required to complete a ring crack on a plate glass was $\frac{1}{2}$ sec, which is similar to that for the present as-received specimen surface.

As indicated above, the Hertzian crack which occurred at P_c already contained a cone portion in addition to the ring, both of which, however, often disappeared upon removal of the load. Therefore, to obtain information on the geometry and extent of the cone, some tests were conducted with a 12.7 mm radius steel ball on a 25 mm thick block in which the load was increased beyond P_c to a value where a cone crack could be clearly detected by eye after unloading. Diametrical sections were then taken through these cracks and they were polished and etched lightly in HF to reveal more clearly the geometry and extent of the crack. Photomicrographs of some typical cracks are given in Fig. 12. They reveal a cone half-angle of approximately 66°. Roesler [8] reported a value of 67.5° ± 1° for the cone half-angle in glass using a cylindrical flat-ended punch, while the results of Mikosza and Lawn [10] (their Fig. 2) suggest a cone angle of 72 to 75°. A cone half-angle of 65.5° was found by Benbow [22] for Hertzian cracks in fused silica; Nadeau [19] reported an angle of 67.5° ± 1° in vitreous carbon.

4.5. Ring crack radius

In accord with the observations of other [3, 9, 17, 18, 20, 23], the ring crack radius r^* in the present tests was greater than the contact radius a calculated using Equation 1. A plot of the ratio r^*/a versus P_c for almost all of the present tests in

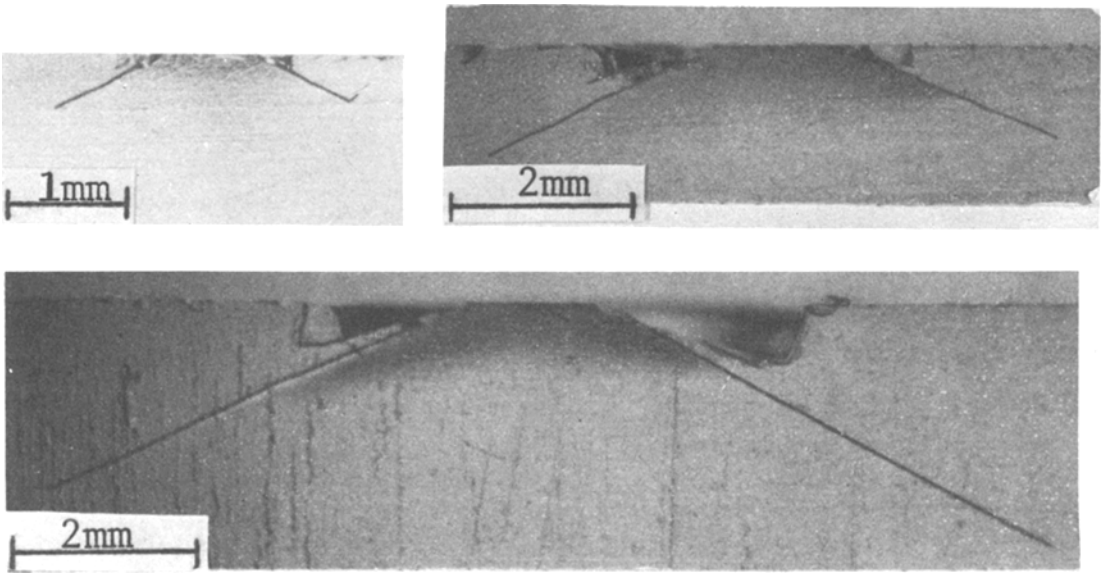

Figure 12 Diametrical sections through Hertzian cracks in as-received Pyrex glass produced with a steel ball of 12.7 mm radius and a velocity of 8.5×10^{-6} m sec^{-1} at loads appreciably greater that P_c. (a) $P = 1.78 \times 10^3$ N, (b) $P = 4.46 \times 10^3$ N, and (c) $P = 8.91 \times 10^3$ N. $P_{c_{0.5}}$ for this ball radius and velocity is 736 N.

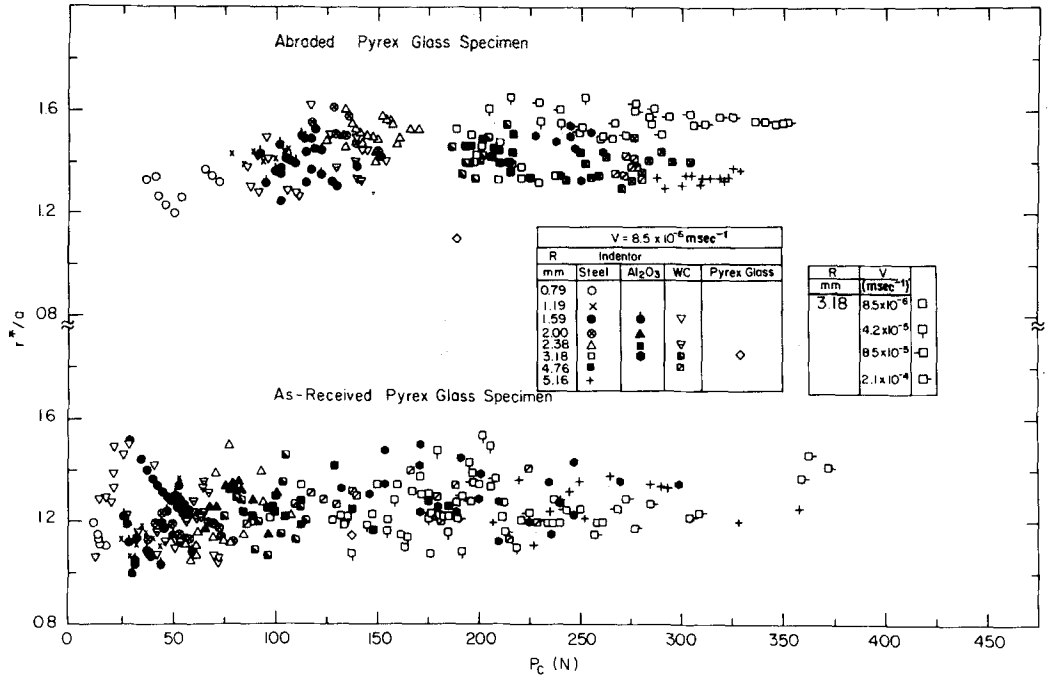

Figure 13 The ratio of the ring crack radius $r^*_{0.5}$ to the contact radius $a_{0.5}$ versus $P_{c0.5}$ for the various conditions investigated.

which the ring crack radius was determined is given in Fig. 13. It should be noted that the ratio for the abraded specimen surface is, in general, higher than that for the as-received surface. However, the ratio for the etched specimen surfaces was nearly the same as for the as-received surface. Also, annealing did not appreciably change the ratio for both the as-received and abraded surfaces.

Several tests were carried out to check whether or not the calculated contact radius agrees with that which actually occurs. For this check the contact radius was measured during the test with the observing microscope employing suitable lighting. Good agreement (within 8%) existed between the measured and calculated values (see Fig. 14).

A log–log plot of r^* versus P_c for the various specimen surfaces and ball materials is presented in Fig. 15. Also included in this plot are the values of the radius of the base of the cone crack r_b obtained from: (a) measurements on the cone crack through the optical microscope as the load was increased stepwise beyond P_c for a number of ball sizes (designated r_{b1}) and (b) measurements on diametrical sections through cone cracks such as those of Fig. 12 produced with a 12.7 mm radius steel ball (designated r_{b2}). To be noted in Fig. 15 is that the data for r^* and r_{b1} for $P_c \leqslant 600$ N can be considered to lie on a single straight line of slope $\frac{2}{3}$, yielding

$$r^*(r_{b1}) = r_0 P^{2/3}, \qquad (7)$$

with $r_0 = 0.93 \times 10^{-5}\,\mathrm{m\,N^{-2/3}}$. The data for the

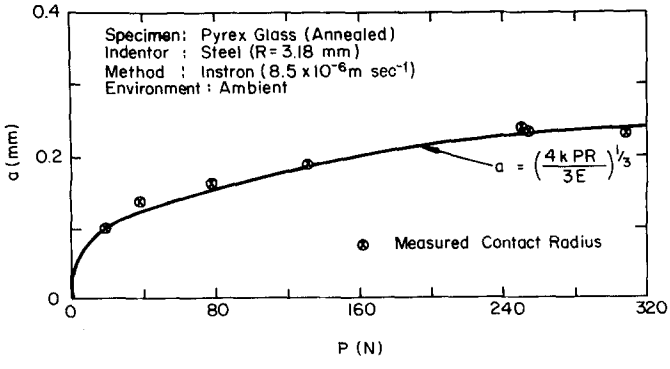

Figure 14 Comparison of the calculated and experimental values of the contact radius a.

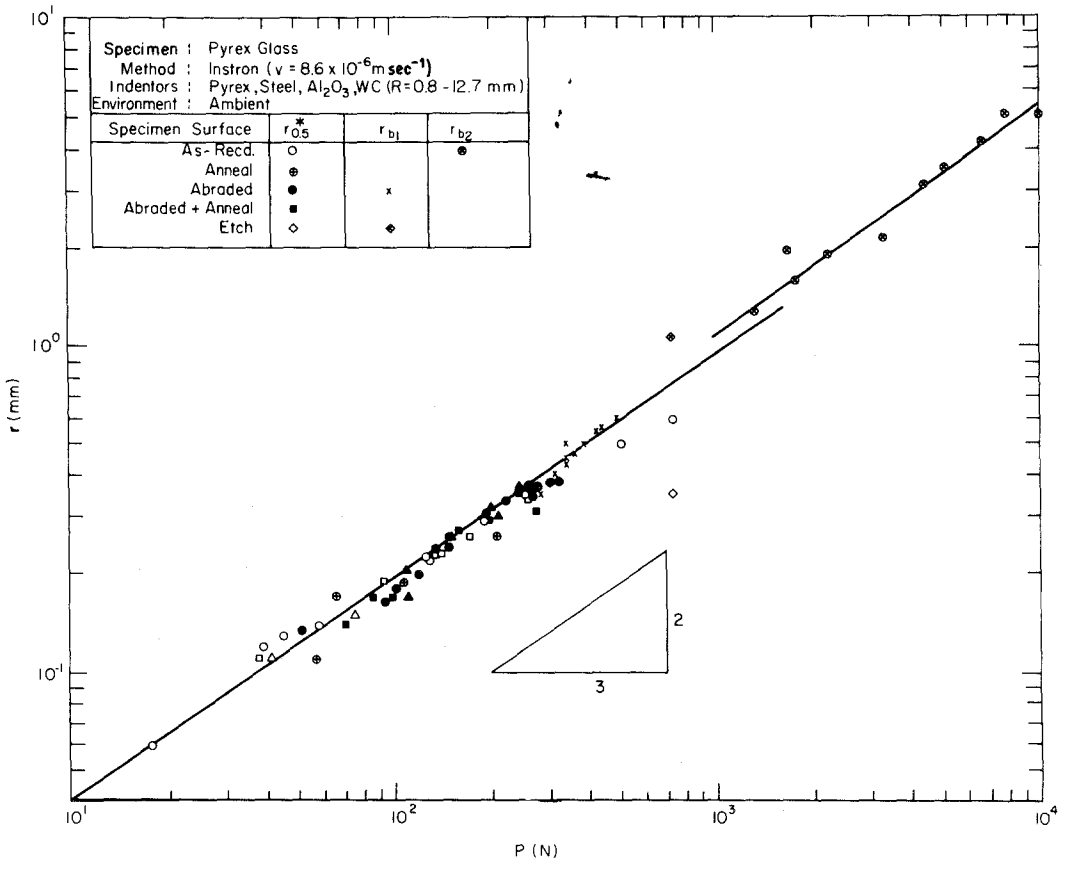

Figure 15 The effect of load for various specimen surface conditions on (a) the ring crack radius $r^*_{0.5}$, (b) the cone crack base radius r_{b_1} viewed through the back side of the specimen, and (c) the cone crack radius r_{b_2} determined by diametrical sectioning.

TABLE VI Effects of environment and lubrication on Hertzian ring crack parameters using a polished steel ball and an indentation rate of 8.5×10^{-6} m sec^{-1}

Indentor radius (mm)	Environment or lubricant	$P_{c0.5}$ (N)	$a_{0.5}$ (mm)	$r^*_{0.5}$ (mm)	$r^*_{0.5}/a_{0.5}$	$P_{c0.5}/R$ (N mm^{-1})	p_0 (MPa)	$\sigma_F^\dagger$ (MPa)
I. Specimen surface: as-received (ground-and-polished)								
3.18	Ambient air	128	0.18	0.22	1.19	40.3	1242	263
4.76	Ambient air	191	0.24	0.29	1.22	40.1	1085	219
3.18	Vacuum (10^{-5} Pa)	300	0.24	0.29	1.19	94.3	1658	354
3.18	Vacuum (10^{-6} Pa)	400	0.27	0.32	1.19	125.8	1813	385
4.76	Silicone grease	308	0.28	0.35	1.26	64.7	1271	240
4.76	Machine oil	302	0.27	0.35	1.28	63.4	1286	235
II. Specimen surface: abraded (400 grit SiC)								
3.18	Ambient air	211	0.21	0.30	1.43	66.4	1467	215
4.76	Ambient air	269	0.27	0.36	1.34	56.5	1216	203
4.76	Silicone grease	455	0.32	0.42	1.33	95.6	1452	246
4.76	Machine oil	550	0.34	0.45	1.34	115.5	1552	259.4

† σ_F = fracture stress = $\left(\frac{1-2\nu}{2}\right) p_0 \left(\frac{a}{r^*}\right)^2$

diametrically sectioned specimens also follow Equation 7, but with $r_0 = 1.05 \times 10^{-5}\,m\,N^{-2/3}$. The slightly larger value of r_0 for the diametrically sectioned specimens is probably due to the fact that the etching employed following sectioning more clearly revealed the total crack length than was the case of the observation under the microscope during a test. That the data for the cone base radius r_{b1} lie on the same curve as those for the ring crack radius, r^*, probably results from the fact that for the most part the cone had not extended appreciably beyond the ring, so that $r_{b1} \approx r^*$.

4.6. Effects of environment and lubrication

Work by Lawn and co-workers [7, 11] indicates that the kinetic effects for Hertzian fracture in ambient air are principally due to the water vapour in the air. To check this, one series of tests was here conducted in a vacuum chamber at two pressures (10^{-5} and 10^{-6} Pa) on the as-received specimen surface using a 3.18 mm radius steel ball and an indentation velocity of $8.5 \times 10^{-6}\,m\,sec^{-1}$. The results of these tests are given in Table VI. It is here seen that P_c increases with decrease in environment pressure, the value at 10^{-6} Pa being about 3 times that at atmospheric pressure. On the other hand, the r^*/a value did not change. The value of P_c/R for the 10^{-6} Pa vacuum is similar to those obtained [23] for free-fall and air rifle tests ($v = 1$ to $10\,m\,sec^{-1}$) on the same specimen, supporting the idea that the kinetic effects observed here (increase in P_c/R with increase in indentor velocity) are principally due to the environment.

To investigate the effect of lubrication on Hertzian crack formation, some tests were carried out with a lubricant applied to both the specimen surface and the ball prior to the test. Two lubricants representing a large difference in viscosity were studied, namely machine oil and silicone stopcock grease. The results for these two lubricants applied to as-received and abraded specimen surfaces are listed in Table VI. It is noted that the effect of the two lubricants is similar, in that they cause an increase in P_c for the constant ball size but do not appreciably alter the value of r^*/a. Also it was found that they did not significantly change the shape of the probability versus P_c distribution curve. Of interest in regard to these tests is that Argon *et al.* [20] reported that the application of machine oil to the surface of window glass had little effect on the Hertzian fracture (presumably no effect on P_c or r^*/a) produced with steel indentors of 2.38 mm radius.

5. Discussion

5.1. Hertzian fracture theories

The more generally known energy balance theories of Hertzian fracture (in contrast to those based on a statistical description of the flaw distribution) are summarized in Table VII. To be noted is that those theories which are based on the original Frank and Lawn [4] type of analysis (Equations 8 to 17) require for a constant flaw size that the critical load for Hertzian ring crack formation be proportional to either the indentor radius R (Auerbach's law) or R^2 (maximum stress criterion for fracture) or to r^{*2}, none of which relations was strictly obeyed for any of the conditions considered in the present investigation. The changes in t_c and $\dot{P}_c$ which occur at a constant indentation rate due to ball size do not appear to be primarily responsible for the lack of agreement. In addition to the problem of the relationship between P_c and R in the Frank and Lawn theory, it is difficult to explain the fact that r^* is greater than a and that the r^*/a ratio varies with surface condition.

The observed proportionality between P_c and $r^{*3/2}$ and between the load P and the cone base radius $r_b^{3/2}$ is in accord with the equation developed by Roesler [8] for the equilibrium growth of Hertzian cone cracks (Equation 9). Using Roesler's equation and taking $\omega = 7.45 \times 10^{-3}$ (derived by Roesler), we obtain $\sim 20\,J\,m^{-2}$ for the surface energy γ_s of the Pyrex glass. This value is 4 to 5 times that obtained by Wiederhorn [24] and Adler [25] for Corning 7740 Pyrex glass using a precracked, double-cantilever beam specimen, suggesting that the value of ω may be too high by this amount for the Pyrex glass and testing conditions employed here. Worthy of note is that values of $\gamma_s \approx 4\,J\,m^{-2}$ were obtained using Roesler's equation for commercial plate glass by Roesler [8] and by Culp [26], both of whom employed a flat-ended cylindrical punch to produce and propagate the cone cracks.

5.2. Friction effects

An important feature of the present results, and those of others, is that the ring crack radius, r^*, is greater than the contact radius, a (where the tensile stress is expected to be a maximum), and that the ratio r^*/a varies with specimen surface condition and with indentor material and its surface

TABLE VII Theories for Hertzian fracture†

Reference	Basis	Flaw dimension	r^*/a	Equation	Equation no.
Roesler [3]	Energy scaling	$c_f \leqslant a$	$\geqslant 1$	$P_c = \frac{5\pi}{2}\frac{\theta}{\eta}\gamma_s R$	8
Roesler [8]	Equilibrium Griffith fracture	$c_f \geqslant a$	$\geqslant 1$	$P_c = \left(\frac{4\pi}{\omega}\frac{\mu\gamma_s}{\sin\alpha}\right)^{1/2} r_b^{3/2}$	9
Frank [4] and Lawn	Fracture mechanics	$c_f < c_0^*$ $c_0^* < 0.02a$	~ 1	$P_c = \left[0.114 + \frac{0.866}{66}\left(\frac{k^2\gamma_s}{E}\right)^{1/2}\frac{R}{c_f^{3/2}}\right]P^*$	10
		$c_0^* < c_f < c^*$ $c^* \approx 0.1a$	~ 1	$P_c = P^* = \frac{8\pi a\sigma_m}{3\delta\sigma'(1-\sigma'/\sigma_m)}\frac{k\gamma_s R}{(1-\nu^2)(1-2\nu)^2}$ $\delta = 0.02a \qquad \sigma = 0.06\sigma_m$	11
		$c_f \gg c^*$	> 1	$P_c \approx 0.5 \times 10^9 c_f^{3/2}$	12
Wilshaw [9]	Fracture mechanics	$c_f \leqslant 3 \times 10^{-2}a$	$\geqslant 1$	$P_c = \left(\frac{32\pi}{3(1.12)^2(1-\nu^2)(1-2\nu)^2}\right)^{3/2}\left(\frac{4}{3E}\right)^{1/2}\left(\frac{\gamma_s}{c_f}\right)^{3/2}\left(\frac{r^*}{a}\right)^6 k^2R^2$ $= \frac{2}{1.12(1-2\nu)}\left(\frac{2\pi\gamma_s E}{1-\nu^2}\right)^{1/2}\frac{r^{*2}}{c_f^{1/2}}$	13a
		$c_f \geqslant 3 \times 10^{-2}a$	$\geqslant 1$	$P_c = \frac{8\pi^3 k\gamma_s R}{27(1-\nu^2)}\left(\frac{a}{c_f}\right)\left[\int_0^{c_f}\frac{\phi_N(y,z)\mathrm{d}z}{(c_f^2-z^2)^{1/2}}\right]^{-2}$	14
Lawn [12] and Wilshaw	Fracture mechanics	$c_f \ll c_0^*$	~ 1	$P_c = \frac{k^2\gamma_s^{3/2}R^2}{\chi(\nu)E^{1/2}c_f^{3/2}}$ $\chi(\nu) = \{3/4\}\,3(1-2\nu)^2(1-\nu^2)/32\pi\}^{1/2}$	15
		$c_0^* \leqslant c_f \leqslant c^*$	~ 1	$P_c = \frac{2k\gamma_s R}{[\phi(c^*/a)]^2}$	16
Evans [33]	Fracture mechanics	$c_f \gg c_0^*$	$\gg 1$	$P_c = \frac{16\pi^3}{27\beta^2}\left(\frac{a}{c_f}\right)kK_I^2R\left[\int_{-c_f/a}^{c_f/a}\frac{w[1+(b/a)/(c_f/a)]}{[(c_f/a)^2-(b/a)^2]^{1/2}}\phi_E\mathrm{d}b\right]^{-2}$ $\beta \approx 1.1; \quad w \approx r^*/b\sin\alpha$	17

c_f = pre-existing flaw size or crack length
a = contact radius
r^* = Hertzian ring crack radius
r_b = radius of the base of a cone crack
P_c = critical load to cause cracking
R = ball radius
$\theta = 2A_c/\pi a^2$; A_c = crack surface area
γ_s = surface energy
η = ratio of fracture energy to total elastic energy
μ = shear modulus
α = cone crack half-angle
ω = constant $\approx 7.45 \times 10^{-3}$
E = Young's modulus
ν, ν' = Poisson ratio of specimen and sphere, respectively
k = Hertzian constant $= \frac{9}{16}\left[(1-\nu^2)+(1-\nu'^2)\frac{E}{E'}\right]$
σ_m = maximum tensile stress $= \left(\frac{1-2\nu}{2}\right)\frac{P}{\pi a^2}$
c_0^* = critical crack size for spontaneous growth of pre-existing flaw into a cone crack
c^* = critical crack size for spontaneous growth of shallow ring crack into a cone crack
$\phi_N, \phi(c^*/a), \phi_E$ = mechanical-energy release rate functions for cone crack formation

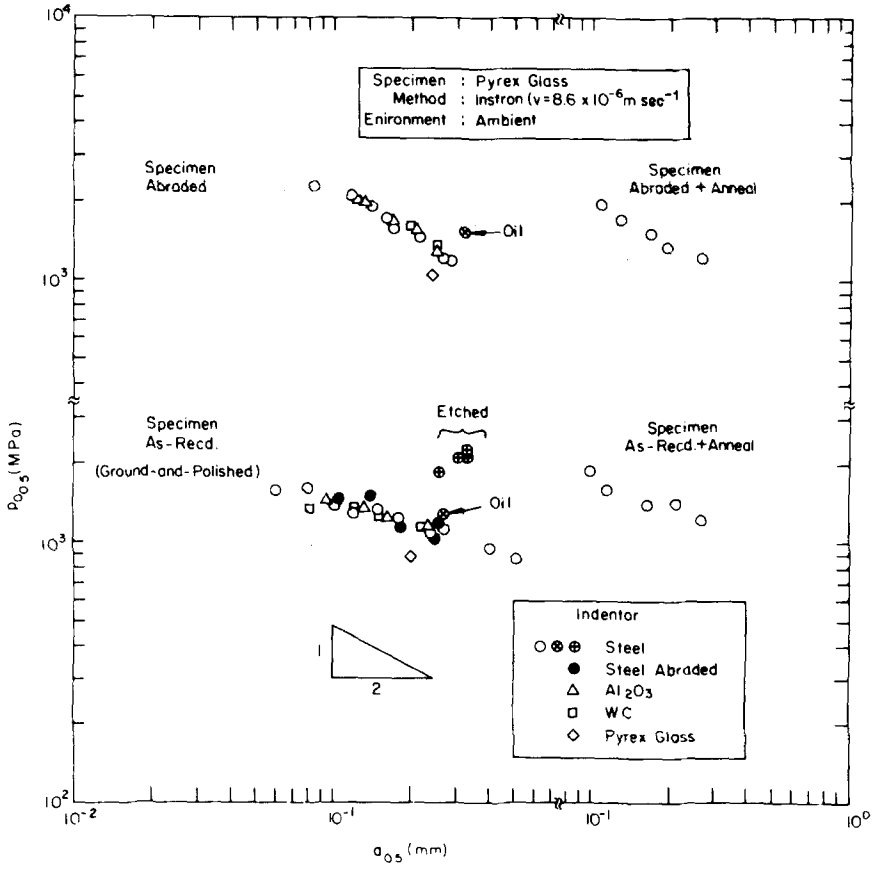

Figure 16 Variation of the average pressure $p_{0\,0.5}$ with the contact radius $a_{0.5}$ for the various specimen surface conditions and indentor materials.

condition. Johnson and *et al.* [27] proposed that friction, which is neglected in the Hertzian fracture theories, is an important factor. They showed that a difference in the elastic properties between the indentor and specimen leads to frictional forces which modify the Hertz distribution of contact stresses and that this modification may be further accentuated upon roughening the indentor or the specimen surface. Of related interest are the observations of Gilroy and Hirst [28], who found that both the critical load for Hertzian fracture and the ball size range for Auerbach's law was significantly influenced by the coefficient of friction between the specimen and the indentor.

As pointed out by Johnson *et al.* [27], the effects of frictional forces are best determined by making comparisons at a constant value of the contact radius a, rather than at a constant indentor size. In such comparisons Auerbach's law yields a proportionality between the average pressure over the contact area $p_0\,(=P/\pi a^2)$ and $a^{-1/2}$. A log–log plot of p_0 versus a is given in Fig. 16 for most of the conditions investigated here. It is here seen that for the as-received specimen surface condition (ground-and-polished) the negative slope is less than $\frac{1}{2}$, while for the abraded surface condition it is greater than $\frac{1}{2}$, again indicating that the present results do not strictly follow Auerbach's law. Of additional interest regarding Fig. 16 is that for the polished steel indentors: (a) p_0 for the abraded specimen surface is higher than that for the as-received surface, and (b) annealing increases p_0 appreciably for the as-received specimen surface but decreases it slightly for the abraded surface. Considering the various indentors, p_0 is essentially the same for the three polished indentor materials (steel, Al_2O_3 and WC), but is significantly less for the Pyrex glass indentor for both the as-received and abraded specimen surface conditions. Abrading the steel indentor increases p_0 slightly.

The variation of the r^*/a ratio with a is shown in Fig. 17. Within the scatter of the data it appears that r^*/a is relatively independent of a for the as-received specimen surface but decreases with a for

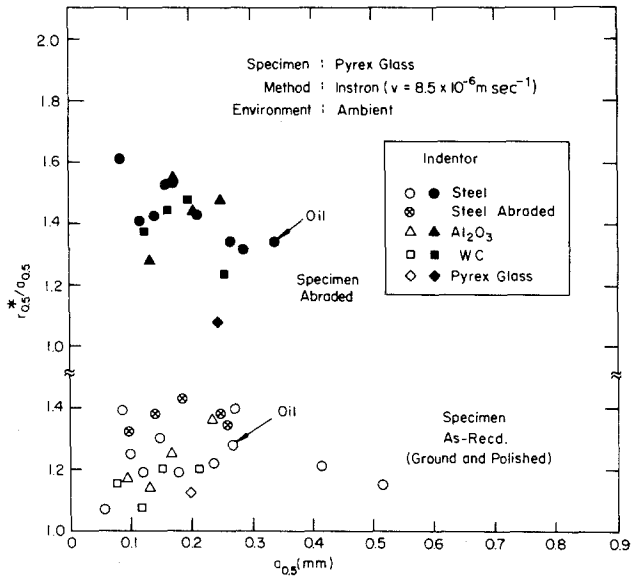

Figure 17 Variation of the ratio $r^*/a_{0.5}$ with the contact radius $a_{0.5}$ for various specimen surface conditions and indentor materials.

the abraded surface. Also, r^*/a is nearly the same for the three indentor materials (steel, Al_2O_3 and WC, all polished) on both the as-received and abraded specimen surfaces, but is decidedly smaller for the Pyrex glass indentor on the abraded specimen surface. Abrading the steel ball increases r^*/a for the as-received specimen surface. Lubrication with oil does not significantly influence the r^*/a ratio.

Of interest is a comparison of the results obtained in the present study with predictions of the friction effects proposed by Johnson *et al.* [27]. Qualitatively, the decrease in p_0 for the Pyrex glass indentor compared to the other materials is in accord with the lower frictional force due to the smaller elastic modulus of the glass. Furthermore, the increase in p_0 upon abrading the specimen (or indentor) surface is expected because of the increased roughness resulting therefrom. Quantitatively, the data of Fig. 16 yield $p_0(\text{steel})/p_0(\text{glass}) = 1.35$ for the as-received specimen surface and polished steel ball. This value is only slightly lower than that ($p_0(\text{steel})/p_0(\text{glass}) = 1.57$) derived from Fig. 2 in the paper of Johnson *et al.* [27] based on the r^*/a values obtained here (Fig. 17) and assuming no friction for the glass ball and a friction traction of $\mu = 0.1$ for the steel ball. Other than experimental error, the lower-than-predicted value for the pressure ratio may be due to a low level roughness of the polished specimen and/or glass ball, which effect would be qualitatively similar to an interfacial friction. That surface roughness may be important is indicated by the fact that even with the polished glass indentor, p_0 for the abraded specimen surface is higher than that for the ground-and-polished surface. Assuming that friction effects are important, the fact that p_0 for the polished steel, Al_2O_3 and WC balls is essentially the same for a constant contact radius would then indicate that the coefficient of friction for these materials is quite similar even though their elastic constants differ (see Table II).

Alternative explanations for the increase in p_0 which occurred upon abrading the as-received specimen surface might be that the abrasion removed: (a) any residual tensile stress which may have originally existed at the surface, and/or (b) any weak "flowed" layer which may have been produced by the grinding-and-polishing operation carried out by the manufacturer. Since the residual stress on the as-received specimen surface is compressive [29], the former explanation does not apply. Also, as will be seen below, calculations of the fracture stress existing at the ring crack radius yield nearly the same values of this stress for the as-received and abraded specimen surfaces, suggesting that any difference in residual stress which may have existed did not significantly influence the results. The relatively constant fracture stress also tends to rule out the possibility that the difference in the behaviour for the two specimen surface conditions is due to the removal of a weak, "flowed" layer at the surface of the as-received material. It therefore appears that the most reason-

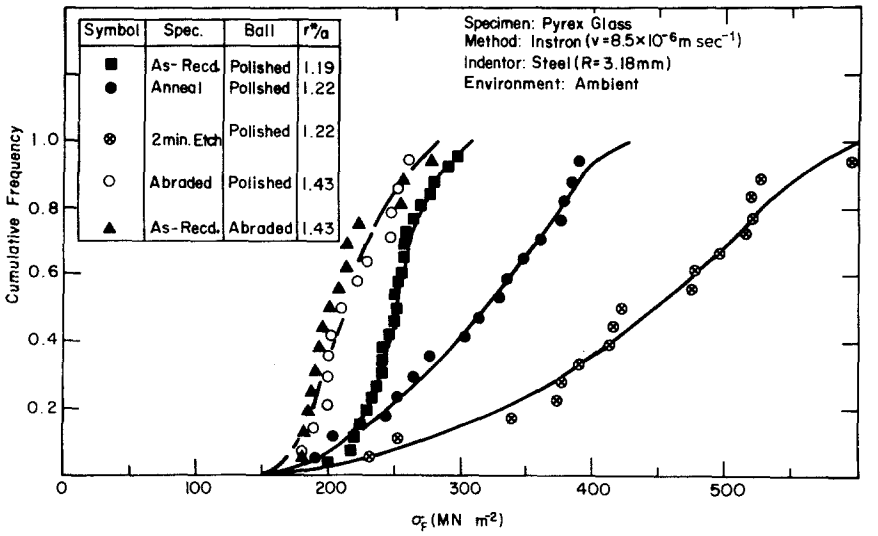

Figure 18 Cumulative frequency versus the fracture stress σ_F at the ring crack radius for various specimen and ball surface conditions. Also listed are the r^*/a values.

able explanation for the difference in p_0 due to the abrasion of the specimen surface is that it results from the increased roughness produced thereby.

An increase in roughness or friction cannot, however, account for the increases in p_0 which resulted upon annealing or etching the as-received specimen surface. The increase in p_0 is much greater than one might expect from any change in roughness produced by these treatments; furthermore, the values of the r^*/a ratio did not change appreciably. It therefore appears that these treatments probably produced a reduction in the density of the more severe flaws.

Further support for the above conclusions is provided by the comparisons presented in Fig. 18, which is a plot of the cumulative frequency versus the fracture stress σ_F at the ring crack radius r^* calculated using Equation 4 for the various specimen and steel ball surface conditions. It is here seen that abrasion of the as-received specimen or indentor surface increases the r^*/a ratio but has little effect on the fracture stress distribution (presumably reflecting the flaw size distribution), whereas annealing or etching of the specimen surface has little, if any, effect on the r^*/a ratio but has a marked influence on the stress distribution.

It is desirable at this point to consider the fact that lubricants such as silicone grease and machine oil caused an increase in p_0, rather than a decrease, without a significant change in the r^*/a ratio. In keeping with the conclusions of Johnson *et al.* [27] , the cleaning procedures employed here are probably not sufficiently rigorous to raise the coefficient of friction above the "boundary lubrication" value. Moreover, at the high contact pressures which occur, the tests with the lubricants would also be under "boundary lubrication" conditions, so that no significant difference in the coefficient of friction is expected. The increase in p_0 due to the presence of these lubricants, therefore, probably results from their influence on the surface energy at the crack tip. This is in accord with the results of Langitan and Lawn [7], who found a significant increase in the critical load for the Hertzian fracture of soda-lime glass for tests under silicone oil compared to air. Similarly, the increase in p_0 for tests under a vacuum (Table VI) and with increase in indentation rate obtained here can be explained in terms of the kinetic effect of water vapour on the surface energy at the crack tip, for it is well known that the strength of glass is significantly reduced by the presence of water vapour and that this effect is time-dependent [7, 30–32].

5.3. Fracture stress

The radial tensile stress σ_F existing at the ring crack radius r^* was calculated using Equation 4 for all of the conditions investigated here at an indentor velocity of 8.5×10^{-6} m sec^{-1} and in ambient air. A log–log plot of σ_F versus r^* is given in Fig. 19. To be noted is that the results obtained in the present investigation scatter about a straight line whose slope is $-\frac{1}{2}$, yielding

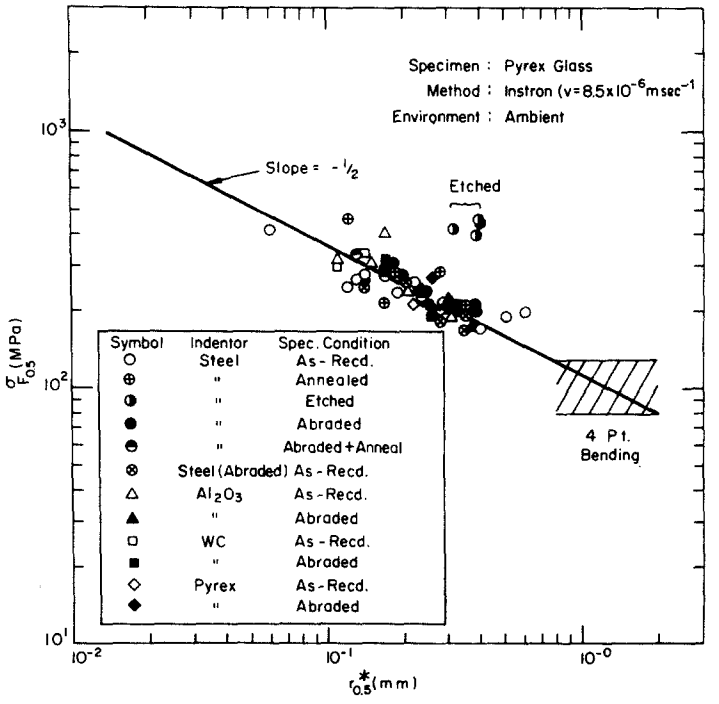

Figure 19 Variation of the fracture stress σ_F at the ring crack radius with $r^*_{0.5}$ for the various specimen surface conditions and indentor materials.

$$\sigma_F = Br^{*-1/2} \tag{18}$$

with $B = 115\,\text{MPa mm}^{1/2}$. Also included in Fig. 19 is the range of values (see Fig. 20) obtained in four-point bend tests conducted at a cross-head speed of $8.5 \times 10^{-6}\,\text{m sec}^{-1}$ under ambient environment on $10 \times 1.25 \times 1.0$ cm specimens prepared from as-received Pyrex glass blocks and from blocks abraded on all surfaces with 400 grit SiC, similar to those used for the Hertzian fracture tests.

The relatively constant value of σ_F for a constant r^* for the as-received and abraded specimen surface conditions, and for the various indentor materials and surface conditions, suggests that any effects due to these factors on P_c and p_0 are mainly due to the roughness and friction effects discussed above. The increase in σ_F with decrease in r^* could then be interpreted to reflect a flaw distribution whose areal density decreases as the severity of the flaw increases. The decrease in scatter in the σ_F values as the ball size increases (see Fig. 21) is in accord with such a flaw size distribution. Also, to be noted from Fig. 19 is that the bend test results correspond to an r^* (and flaw spacing) of about 1 mm, which is in reasonable accord with the observed variation in distance of the fracture from the position of maximum stress at the bend specimen surface.

Assuming that the maximum flaw size in the abraded bend specimens was 18 μm and taking the applicable fracture toughness relation [9]

$$\sigma_F = \frac{1}{1.12}\left(\frac{2E\gamma_s}{(1-\nu^2)\pi c_f}\right)^{1/2}, \tag{19}$$

where c_f is the crack length, one obtains $\gamma_s = 4.2\,\text{J m}^{-2}$ for the surface energy of the Pyrex glass upon taking the smallest fracture stress given in Fig. 20 for the abraded specimen. This value of γ_s is in good accord with that (4.0 to $4.6\,\text{J m}^{-2}$) obtained by others [24, 25] with a pre-cracked,

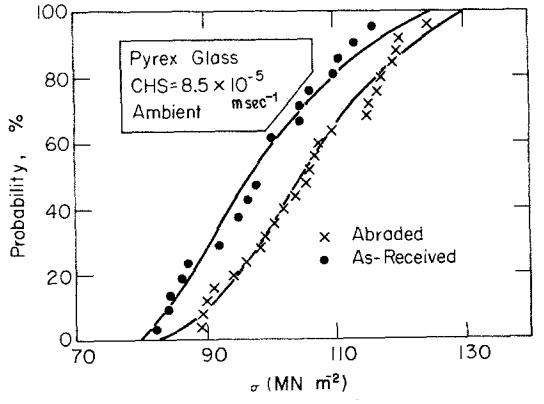

Figure 20 Probability of fracture versus the fracture stress in four-point bending for as-received and abraded surfaces of Pyrex glass.

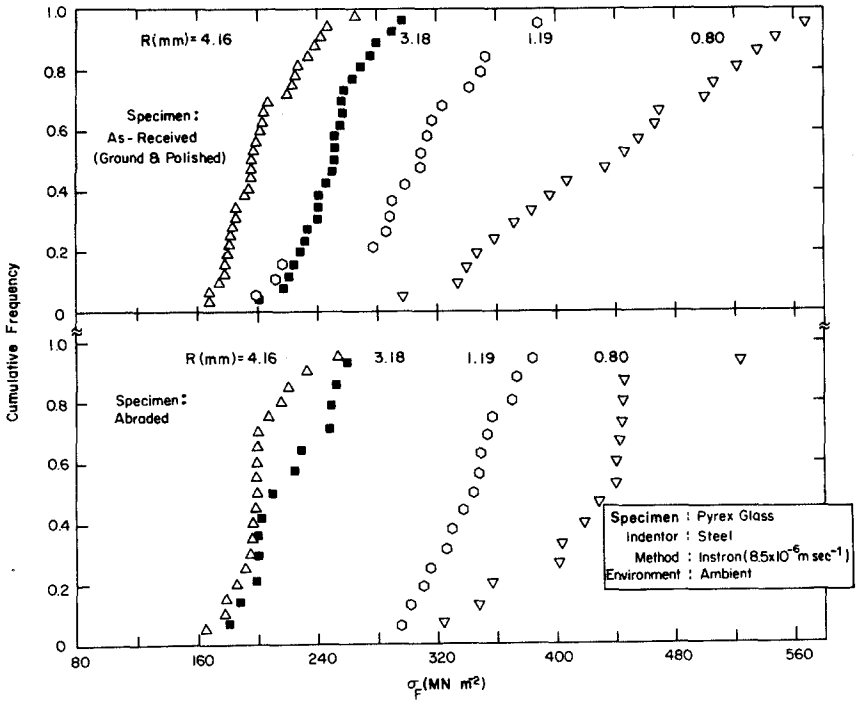

Figure 21 Effect of ball size on the probability of fracture versus σ_F for as-received and abraded specimen surfaces.

double-cantilever beam test specimen. Knowing γ_s we can calculate the maximum crack length for the as-received surface from the fracture stress in bending for this surface condition. The maximum crack length so obtained is 16 μm, which is not appreciably different from that for the abraded surface. Similar calculations for the steel indentors of 0.79 to 12.7 mm radius give $c_f = 0.6$ to 3.5 μm for the as-received and abraded specimen surfaces. Values of $c_f = 0.7$ to 1.0 μm were obtained for the etched specimen surface using the 3.18 mm radius steel ball.

Upon combining Equations 18 and 19 with Equation 13a (Wilshaw's theory), we obtain $P_c = \text{const.}\, r^{*3/2}$, in accord with the results of Fig. 15. Further, upon taking B of Equation 18 equal to 115 MPa mm$^{1/2}$, one obtains $P_c^2/r^{*3} = 1.45 \times 10^{15}$ N^2 m^{-3}. This value is in reasonable accord with the value of 1.25×10^{15} N^2 m^{-3} determined directly from Fig. 15.

The above considerations lead to the conclusion that Hertzian fracture in Pyrex glass occurs by the direct, unstable propagation into a cone crack of a pre-existing surface flaw in the vicinity of the maximum tensile stress. The location of the maximum tensile stress is determined by surface roughness and friction, but its value for conditions considered here appears to be not much different from that given by the Hertz equation for that position. Further, the nature of the flaw distribution is such that Hertzian fracture results from smaller cracks as the indentor size decreases. Quantitative estimates yield a value of ~ 4 J m^{-2} for the surface energy of Pyrex glass in ambient air, and yield flaw sizes responsible for the Hertzian fracture of the order of 0.5 to 4 μm. The length of the cone crack and its growth are described by Roesler's equation, but his derived constant appears to be too high by a factor of 5.

6. Conclusions

The effects of (a) specimen surface condition, (b) indentor size, material and surface condition, (c) speed of testing and (d) environment (including lubrication) on the Hertzian fracture of Pyrex glass were investigated using an Instron machine. The following is a summary of the experimental results obtained:

(1) In keeping with the behaviour of brittle materials, the data exhibited considerable scatter. The values of the parameters considered here were those at a cumulative frequency of 0.5.

(2) The results were not in strict accord with Auerbach's law.

(3) The ring crack radius r^* was always greater than the contact radius a. The r^*/a ratio was

relatively independent of ball material and size, but increased with specimen and indentor surface roughness.

(4) The ring crack radius was proportional to the critical load $P_c^{2/3}$, relatively independent of: (a) surface condition of the specimen and (b) indentor material and surface condition. A similar relation was found for the cone crack base radius determined by diametrical sectioning.

(5) An increase in the speed of testing, the application of lubricants and testing in a vacuum all lead to an increase in P_c for a given ball size.

(6) The fracture stress taken at the fracture site increases with decrease in r^*, being approximately proportional to $r^{*-1/2}$.

The conclusions reached regarding these results are:

(1) The variations in r^*/a with specimen and indentor conditions are due to the effects of surface roughness and friction as proposed by Johnson *et al.* As a result, the maximum tensile stress at the surface occurs at r^* rather than at the contact radius a.

(2) Hertzian fracture occurs by the direct, unstable growth of a pre-existing flaw into a fully developed cone crack according to the usual fracture mechanics relations, similar to the theory proposed by Wilshaw.

(3) The flaw size c_f responsible for the fracture decreases with indentor size, i.e. with a or r^*. The experimental results indicate that $c_f \alpha r^{*1/2}$.

(4) A surface energy γ_s of 4.2 J m^{-2} was derived from bend tests on specimens with similar surface conditions as for the Hertzian fracture tests. Using this value of γ_s, the crack sizes which lead to fracture ranged between 0.6 and 3.5 μm for the ball size range of 0.9 to 12.7 mm radius and specimen and indentor surface conditions considered here.

(5) The proportionality of r^* and of the base of the cone crack r_b with $P_c^{2/3}$ suggests that the length of the initial cone crack and its growth are described reasonably will by Roesler's theory; however, his constant appears to be too high by a factor of about 5.

(6) The increase in critical load with speed of testing, with lubricants, and upon testing in a vacuum are due to kinetics effects associated with the influence of the environment on the crack growth, i.e. the effect of environment on the surface energy γ_s at the crack tip. It is concluded that the controlling gas species in air is water vapour.

Acknowledgement

This material is based upon work supported by the National Science Foundation under Grant no. DMR 75-10347.

References

1. H. HERTZ, *J. Reine Angew. Math.* **92** (1881) 156; *Vehandlungen des Vereins zur Beforderung des Gewerbe Fleisses*, **61** (1882) 449; reprinted in English, "Hertz's Miscellaneous Papers" (MacMillan, London, 1896) ch. 5 and 6.
2. F. AUERBACH, *Ann. Phys. Chem.* **43** (1891) 61.
3. F. C. ROESLER, *Proc. Phys. Soc.* **69B** (1956) 981.
4. F. C. FRANK and B. R. LAWN, *Proc. Roy. Soc.* **299A** (1967) 291.
5. B. R. LAWN, *J. Appl. Phys.* **39** (1968) 4828.
6. F. B. LANGITAN and B. R. LAWN, *ibid* **40** (1969) 4009.
7. *Idem, ibid* **41** (1970) 3357.
8. F. C. ROESLER, *Proc. Phys. Soc.* **69B** (1956) 981.
9. T. R. WILSHAW, *J. Phys.* **4** (1971) 1567.
10. A. G. MIKOSZA and B. R. LAWN, *J. Appl. Phys.* **42** (1971) 5540.
11. M. SWAIN, T. WILLIAMS, B. LAWN and T. BEEK, *J. Mater. Sci.* **8** (1973) 1153.
12. B. R. LAWN and R. WILSHAW, *ibid* **10**, (1975) 1049.
13. A. G. EVANS and T. R. WILSHAW, *Acta. Met.* **24** (1976) 939.
14. A. S. ARGON, *Proc. Roy. Soc.* **250A** (1959) 472.
15. J. P. A. TILLETT, *Proc. Phys. Soc. London Sect. B* **60** (1956) 55.
16. H. L. OH and I. FINNIE, *J. Mech. Phys. Solids* **18** (1967) 401.
17. B. HAMILTON and H. RAWSON, *ibid* **18** (1970) 127.
18. J. S. NADEAU and A. S. RAO, *J. Canad. Ceram. Soc.* **41** (1972) 63.
19. J. S. NADEAU, *J. Amer. Ceram. Soc.* **56**, (1973) 467.
20. A. S. ARGON, Y. HARIL and E. OROWAN, *ibid* **43** (1960) 86.
21. J. P. ANDREWS, *Phys. Soc. London* **75** (1970) 697.
22. J. J. BENBOW, *ibid* **75** (1960) 697.
23. J. LU, Y. CHEN, G. SARGENT and H. CONRAD, unpublished research, University of Kentucky (1977).
24. S. M. WIEDERHORN, *J. Amer. Ceram. Soc.* **52** (1969) 99.
25. W. F. ADLER, Air Force Materials Lab. Rept. no. 4, F. 33615-73-C-5057 May (1975).
26. C. J. CULP, *J. Soc. Glass Technol.* **41** (1957) 157.
27. K. L. JOHNSON, J. J. O'CONNOR and A. C. WOODWARD, *Proc. Roy. Soc. London* **A293** (1972) 710.
28. D. R. GILROY and W. HIRST, *Brit. J. Appl. Phys. (J. Phys. D.) Ser. 2* **2** (1969) 1784.
29. SALLY D. SCAPTURA, Corning Co, private communication (1978).
30. T. C. BAKER and F. W. PRESTON, *J. Appl. Phys.*

17 (1945) 170, 179.
31. R. J. CHARLES, *ibid* **29** (1958) 1554.
32. R. E. MOULD, *J. Amer. Ceram. Soc.* **44** (1961) 481.
33. A. G. EVANS, *ibid* **56** (1973) 405.
34. A. K. LYLE, "Glass Compositions", Handbook of Glass Manufacturing, Vol. 1, edited by F. V. Tooley (Ogden, New York) (1974) p. 3.

Received 25 September and accepted 12 October 1978.